DOCTORAT BRETAGNE LOIRE / MATIERE MOLECULES ET MATERIAUX

UNIVERSITÉ DE NANTES

1

2

THÈSE DE DOCTORAT DE

L'UNIVERSITÉ DE NANTES

ÉCOLE DOCTORALE N° 596
Matière, Molécules, Matériaux
Spécialité : *Physique des particules*

Par
Léonard Imbert

Precision measurement of solar neutrino oscillation parameters with the JUNO small PMTs system and test of the unitarity of the PMNS matrix

Thèse présentée et soutenue à Nantes, le Too soon and too early at the same time
Unité de recherche : Laboratoire SUBATECH, UMR 6457

Rapporteurs avant soutenance :

Someone	Very high position, Somewhere
Someone else	Another high position, Somewhere else

Composition du Jury :

Président :	Jacques Chirac	French president, France
Examinateurs :	Yoda	Master, Dagobha
Dir. de thèse :	Frédéric Yermia	Professeur, Université de Nantes
Co-dir. de thèse :	Benoit Viaud	Chargé de recherche, CNRS

Invité(s) :

Victor Lebrin	Docteur, CNRS/SUBATECH

List of Abbreviations

ACU	**A**utomatic **C**alibration **U**nit
CD	**C**entral **D**etector
CLS	**C**able **L**oop **S**ystem
GT	**G**uiding **T**ube
IBD	**I**nverse **B**eta **D**ecay
IO	**I**nverse **O**rdering
JUNO	**J**iangmen **U**nderground **N**eutrino **O**bservatory
LPMT	**L**arge **PMT**
LS	**L**iquid **S**cintillator
NMO	**N**eutrino **M**ass **O**rdering
NO	**N**ormal **O**rdering
PE	**P**hoto **E**lectron
PMT	**P**hoto-**M**ultipliers **T**ubes
ROV	**R**emotely **O**perated under-LS **V**ehicle
SPMT	**S**mall **PMT**
TR Area	**T**otal **R**eflexion **Area**
TTS	**T**ime **T**ransit **S**pread
TT	**T**op **T**racker
WCD	**W**ater **C**herenkov **D**etector

Contents

Remerciements

Introduction

Chapter 1

Neutrino physics

The neutrino, or ν for the close friends, a fascinating and invisible particle. Some will say that dark matter also have those property but at least we are pretty confident that neutrinos exists.

1.1 Standard model

Decrire le m
Regarder th
Kochebina
Limite du m
Interessant,
les neutrino
CP ? Pb des

1.1.1 Limits of the standard model

1.2 Historic of the neutrino

First theories

Discovery

Milestones and anomalies

1.3 Oscillation

1.3.1 Phenomologies

1.4 Open questions

Chapter 2

The JUNO experiment

"Ave Juno, rosae rosam, et spiritus rex". It means nothing but I found it in tone.

The first idea of a medium baseline (∼52 km) experiment, was explored in 2008 [1] where it was demonstrated that the Neutrino Mass Ordering (NMO) could be determined by a medium baseline experiment if $\sin^2(2\theta_{13}) > 0.005$ without the requirements of accurate knowledge of the reactor antineutrino spectra and the value of Δm^2_{32}. From this idea is born the Jiangmen Underground Neutrino Observatory (JUNO) experiment.

JUNO is a neutrino detection experiment under construction located in China. Its main objectives are the determination of the mass ordering at the 3-4σ level in 6 years of data taking and the measurement at the sub-percent precision of the oscillation parameters Δm^2_{21}, $\sin^2\theta_{12}$, Δm^2_{32} and with less precision $\sin^2\theta_{13}$[2].

FIGURE 2.1 – **On the left:** Location of the JUNO experiment and its reactor sources in southern china. **On the right:** Aerial view of the experimental site

For this JUNO will measure the electronic anti-neutrinos ($\bar{\nu}_e$) flux coming from the nuclear reactors of Taishan, Yangjiang, for a total power of 26.6 GW$_{th}$, and the Daya Bay power plant to a lesser extent. Details about the power plants and there expected flux of $\bar{\nu}_e$ can be found in the table 2.1. The distance of 53 km has been specifically chosen to maximize the disappearance probability of the $\bar{\nu}_e$.

2.1 Neutrinos physics in JUNO

Even if JUNO design (section 2.2) was optimized for the measurement of the NMO, its large detection volume, excellent energy resolution and background level and understanding make it also an excellent detector to measure the flux coming from other neutrino sources. Thus the scientific program of JUNO extends way over reactor antineutrinos. The following section is an overview of the different physics topic JUNO will contribute in the coming years.

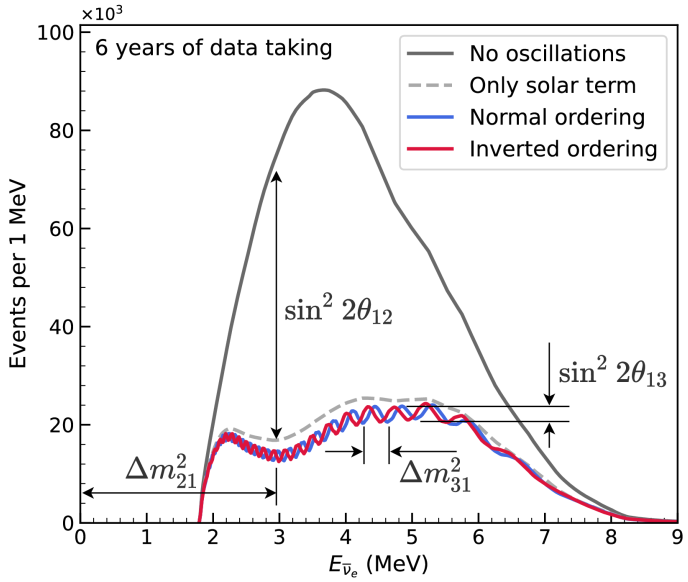

FIGURE 2.2 – Expected number of neutrinos event per MeV in JUNO after 6 years of data taking. The black curve shows the flux if there was no oscillation. The light gray curve shows the oscillation if only the solar terms are taken in account (θ_{12}, Δm^2_{21}). The blue and red curve shows the spectrum in the case of, respectively, NO and IO. The dependency of the oscillation to the different parameters are schematized by the double sided arrows. We can see the NMO sensitivity by looking at the fine phase shift between the red and the blue curve.

2.1.1 Reactor neutrino oscillation for NMO and precise measurements

Previous works [1, 3] shows that oscillation parameters and the NMO can be observed by looking at the $\bar{\nu}_e$ disappearance spectrum coming from medium baseline nuclear reactor. This disappearance probability can be expressed as [2] :

$$P(\bar{\nu}_e \to \bar{\nu}_e) = 1 - \sin^2 2\theta_{12} c_{13}^4 \sin^2 \frac{\Delta m^2_{21} L}{4E} - \sin^2 2\theta_{13} \left[c_{12}^2 \sin^2 \frac{\Delta m^2_{31} L}{4E} + s_{12}^2 \sin^2 \frac{\Delta m^2_{32} L}{4E} \right]$$

Where $s_{ij} = \sin\theta_{ij}$, $c_{ij} = \cos\theta_{ij}$, E is the $\bar{\nu}_e$ energy and L is the baseline. We can see the sensitivity to the NMO in the dependency to Δm^2_{32} and Δm^2_{31} causing a phase shift of the spectrum as we can see in the figure 2.2. By carefully fitting this spectrum, one can extract the NMO and the oscillation parameters. The fit is reviewed in more details in the section 2.6.1. To reach the desired sensitivity, JUNO must meet multiple requirements but most notably:

1. An energy resolution of $3\%/\sqrt{E(\mathrm{MeV})}$ to be able to distinguish the fine structure of the fast oscillation.
2. An energy precision of 1% in order to not err on the location of the oscillation pattern.
3. A baseline of 53 ± 0.5 km to maximise the $\bar{\nu}_e$ oscillation probability.
4. At least $\approx$ 100,000 events to limit the spectrum distortion dur to statistical uncertainties.

$\bar{\nu}_e$ flux coming from nuclear power plants

To get such high measurements precision, it is necessary to have a very good understanding of the sources characteristics. For its NMO and precise measurement studies, JUNO will observe the energy spectrum of neutrinos coming from the nuclear power plants Taishan and Yangjiang's cores, located at 53 km of the detector to maximise the disappearance probability of the $\bar{\nu}_e$.

Reactor	Power (GW$_{th}$)	Baseline (km)	IBD Rate (day^{-1})	Relative Flux (%)
Taishan	9.2	52.71	15.1	32.1
Core 1	4.6	52.77	7.5	16.0
Core 2	4.6	52.64	7.6	16.1
Yangjiang	17.4	52.46	29.0	61.5
Core 1	2.9	52.74	4.8	10.1
Core 2	2.9	52.82	4.7	10.1
Core 3	2.9	52.41	4.8	10.3
Core 4	2.9	52.49	4.8	10.2
Core 5	2.9	52.11	4.9	10.4
Core 6	2.9	52.19	4.9	10.4
Daya Bay	17.4	215	3.0	6.4

TABLE 2.1 – Characteristics of the nuclear power plants observed by JUNO. The IBD rate are estimated from the baselines, the reactors full thermal power, selection efficiency and the current knowledge of the oscillation parameters

The $\bar{\nu}_e$ coming from reactors are emitted from β-decay of unstable fission fragments. The Taishan and Yangjiang reactors are pressurised water reactor (PWR), the same type as Daya Bay. In those type of reactor more the 99.7 % and $\bar{\nu}_e$ are produced by the fissions of four fuel isotopes ^{235}U, ^{238}U, ^{239}Pu and ^{241}Pu. The neutrino flux per fission of each isotope is determined by the inversion of the measured β spectra of fission product [4–8] or by calculation using the nuclear databases [9, 10]. The neutrino flux coming from a reactor at a time t can be predicted using

$$\phi(E_\nu, t)_r = \frac{W_{th}(t)}{\sum_i f_i(t) e_i} \sum_i f_i(t) S_i(E_\nu) \tag{2.1}$$

where $W_{th}(t)$ is the thermal power of the reactor, $f_i(t)$ is the fraction fission of the ith isotope, e_i its thermal energy released in each fission and $S_i(e_\nu)$ the neutrino flux per fission for this isotope. Using this method, the flux uncertainty is expected to be of an order of 2-3 % [11].

In addition to those prediction, a satellite experiment named TAO[12] will be setup near the reactor core Taishan-1 to measure with an energy resolution of 2% at 1 MeV the neutrino flux coming from the core. It will help identifying unknown fine structure and give more insight on the $\bar{\nu}_e$ flux coming from this reactor.

One the open issue about reactor anti-neutrinos flux is the so-called neutrino anomaly [13], an unexpected surplus of neutrino emission in the spectra around 5 MeV. Multiples scientists are trying to explain this surplus by advanced recalculation of the nuclei model during beta decay [14, 15] but no consensus on this issue has been reached yet.

Background in the neutrinos reactor spectrum

Considering the close reactor neutrinos flux as the main signal, the signals that are considered as background are:

— The geoneutrinos producing background in the 0.511 $\sim$ 2.7 MeV region.

— The neutrinos coming from the other nuclear reactors around Earth.

In addition to all those physics signal, non-neutrinos signal that would mimic an IBD will also be present. It is composed of:

— The signal coming from radioactive decay (α, γ, β) from natural radioactive isotopes in the material of the detector.

— Cosmogenic event such as fast neutrons and activated isotopes induced by muons passing through the detector, most notably the spallation on ^{12}C.

All those events represent a non-negligeable part of the spectrum as shown in figure 2.3.

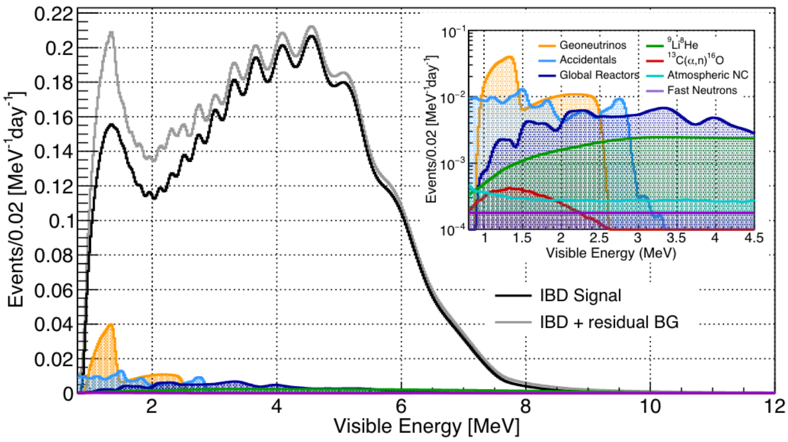

FIGURE 2.3 – Expected visible energy spectrum measured with the LPMT system with (grey) and without (black) backgrounds. The background amount for about 7% of the IBD candidate and are mostly localized below 3 MeV [11]

Identification of the mass ordering

To identify the mass ordering, we fit the neutrino energy spectrum under the two hypothesis of NO and IO. Those two fit give us two χ^2, respectively χ^2_{NO} and χ^2_{IO}. By computing the difference $\Delta\chi^2 = \chi^2_{NO} - \chi^2_{IO}$ we can determine the most probable mass ordering: NO if $\Delta\chi^2 > 0$ and IO if $\Delta\chi^2 < 0$. Current studies shows that the expected sensitivity the mass ordering would be of 3.4σ after 6 years of data taking in nominal setup[2]. More detailed explanations about the fitting procedure can be found in the section 2.6.1.

Precise measurement of the oscillations parameters

The oscillations parameters θ_{12}, θ_{13}, Δm^2_{21}, Δm^2_{31} are free parameters in the fit of the oscillation spectrum. The precision on those parameters have been estimated and are shown in table 2.2. Wee see that for θ_{12}, Δm^2_{21}, Δm^2_{31}, precision at 6 years is better than the reference precision by an order of magnitude [11]

	Central Value	PDG 2020	100 days	6 years	20 years
$\Delta m^2_{31}\,(\times 10^{-3}\mathrm{eV}^2)$	2.5283	$\pm$0.034 (1.3%)	$\pm$0.021 (0.8%)	$\pm$0.0047(0.2%)	$\pm$0.0029(0.1%)
$\Delta m^2_{21}\,(\times 10^{-3}\mathrm{eV}^2)$	7.53	$\pm$0.18 (2.4%)	$\pm$0.074 (1.0%)	$\pm$0.024(0.3%)	$\pm$0.017(0.2%)
$\sin^2\theta_{12}$	0.307	$\pm$0.013 (4.2%)	$\pm$0.0058 (1.9%)	$\pm$0.0016(0.5%)	$\pm$0.0010(0.3%)
$\sin^2\theta_{13}$	0.0218	$\pm$0.0007 (3.2%)	$\pm$0.010 (47.9%)	$\pm$0.0026(12.1%)	$\pm$0.0016(7.3%)

TABLE 2.2 – A summary of precision levels fir the oscillation parameters. The reference value (PDG 2020 [16]) is compared with 100 days, 6 years and 20 years of JUNO data taking.

2.1.2 Other physics

While the design of JUNO is tailored to measure $\bar{\nu}_e$ coming from nuclear reactor, JUNO will be able to detect neutrinos coming from other sources thus allowing for a wide range of physics studies as detailed in the table 2.3 and in the following sub-sections.

Research	Expected signal	Energy region	Major backgrounds
Reactor antineutrino	60 IBDs/day	0–12 MeV	Radioactivity, cosmic muon
Supernova burst	5000 IBDs at 10 kpc	0–80 MeV	Negligible
	2300 elastic scattering		
DSNB (w/o PSD)	2–4 IBDs/year	10–40 MeV	Atmospheric ν
Solar neutrino	hundreds per year for ^{8}B	0–16 MeV	Radioactivity
Atmospheric neutrino	hundreds per year	0.1–100 GeV	Negligible
Geoneutrino	$\approx$ 400 per year	0–3 MeV	Reactor ν

TABLE 2.3 – Detectable neutrino signal in JUNO and the expected signal rates and major background sources

Geoneutrinos

Geoneutrinos designate the antineutrinos coming from the decay of long-lived radioactive elements inside the Earth. The 1.8 MeV threshold necessary for the IBD makes it possible to measure geoneutrinos from ^{238}U and ^{232}Th decay chains. The studies of geoneutrinos can help refine the Earth crust models but is also necessary to characterise their signal, as they are a background to the mass ordering and oscillations parameters studies.

Atmospheric neutrinos

Atmospheric neutrinos are neutrinos originating from the decay of π and K particles that are produced in extensive air showers initiated by the interactions of cosmic rays with the Earth atmosphere. Earth is mostly transparent to neutrinos below the PeV energy, thus JUNO will be able to see neutrinos coming from all directions. Their baseline range is large (15km $\sim$ 13000km), they can have energy between 0.1 GeV and 10 TeV and will contain all neutrino and antineutrinos flavour. Their studies is complementary to the reactor antineutrinos and can help refine the constraints on the NMO [2].

Supernovae burst neutrinos

Neutrinos are crucial component during all stages of stellar collapse and explosion. Detection of neutrinos coming for core collapse supernovae will provide us important informations on the mechanisms at play in those events. Thanks to its 20 kt LS, JUNO has excellent capabilities to detect all flavour of the $\mathcal{O}$(10 MeV) postshock neutrinos, and using neutrinos of the $\mathcal{O}$(1 MeV) will give informations about the pre-supernovae neutrinos. All those informations will allow to disentangle between the multiple hydro-dynamic models that are currently used to describe the different stage of core-collapse supernovae.

Diffuse supernovae neutrinos background

Core-collapse supernovae in our galaxy are rare events, but they frequently occur throughout the visible Universe sending burst of neutrinos in direction of the Earth. All those events contributes to a low background flux of low-energy neutrinos called the Diffuse Supernovae Neutrino Background (DSNB). Its flux and spectrum contains informations about the red-shift dependent supernovae rate, the average supernovae neutrino energy and the fraction of black-hole formation in core-collapse supernovae. Depending of the DSNB model, we can expect 2-4 IBD events per year in the energy range above the reactor $\bar{\nu}_e$ signal, which is competitive with the current Super-Kamiokande+Gadolinium phase [17].

Beyond standard model neutrinos interactions

JUNO will also be able to probe for beyond standard model neutrinos interactions. After the main physics topics have been accomplished, JUNO could be upgraded to probe for neutrinoless beta decay ($0\nu\beta\beta$). The detection of such event would give critical informations about the nature of neutrinos, is it a majorana or a dirac particle. JUNO will also be able to probe for neutrinos that would come for the decay or annihilation of Dark Matter inside the sun and neutrinos from putative primordial black hole. Through the unitary test of the mixing matrix, JUNO will be able to search for light sterile neutrinos. Thanks to JUNO sensitivity, multiple other exotic can be performed on neutrino related beyond standard model interactions.

2.2 The JUNO detector

The JUNO detector is a scintillator detector buried 693.35 meters under the ground (1800 meters water equivalent). It consist of Central Detector (CD), a water pool and a Top Tracker (TT) as showed in figure 2.4a The CD is an acrylic vessel containing the 20 ktons of LS. It is supported by a stainless steel structure and is immersed in that water pool that is used as shielding from external radiation and as a cherenkov detector for the background. The top of the experiment is partially covered by the TT, a plastic scintillator detector which is use to detect the atmospheric muons background acting as veto detector.

The top of the experiment also host the LS purification system, a water purification system, a ventilation system to get rid of the potential radon in the air. The CD is observed by two system of Photo-Multipliers Tubes (PMT). They are attached to the steel structure and their electronic readout is submersed near them. A third system of PMT is also installed on the structure but are facing outward of the CD, instrumenting the water to be cherenkov detector. The CD and the cherenkov detector are optically separated by Tyvek sheet. A chimney for LS filling and purification and for calibration operations connects the CD to the experimental hall from the top.

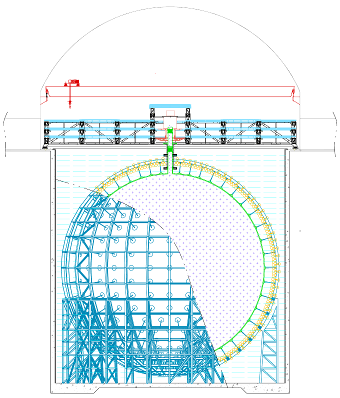

(A) Schematics view of the JUNO detector.

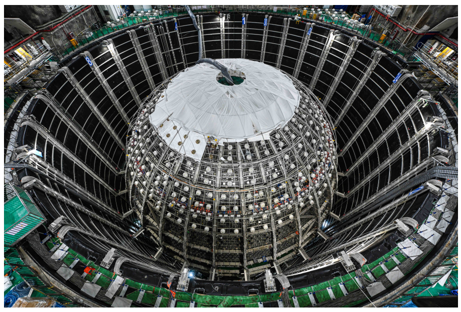

(B) Top down view of the JUNO detector under construction

This section cover in details the different components of the detector and the detection systems.

2.2.1 Principle of detection

The CD will detect the neutrino and measure their energy mainly via an Inverse Beta Decay (IBD) interaction with proton (mainly ^{12}C and H) in the LS:

$$\bar{\nu}_e + p \rightarrow n + e^+$$

Kinematics calculation shows that this interaction has an energy threshold for the $\bar{\nu}_e$ of $(m_n + m_e - m_p) \approx 1.806$ MeV [18] where m_λ is the mass of the λ particle. This threshold make the experiment blind to very low energy neutrinos. The residual energy $E_\nu - 1.806$ MeV is be distributed as kinetic energy between the positron and the neutron. The energy of the emitted positron E_e is given by [18]

$$E_e = \frac{(E_\nu - \delta)(1+\epsilon_\nu) + \epsilon_\nu \cos\theta \sqrt{(E_\nu - \delta)^2 + \kappa m_e^2}}{\kappa} \tag{2.2}$$

where $\kappa = (1+\epsilon_\nu)^2 - \epsilon_\nu^2 \cos^2\theta \approx 1$, $\epsilon_\nu = \frac{E_\nu}{m_p} \ll 1$ and $\delta = \frac{m_n^2 - m_p^2 - m_e^2}{2m_p} \ll 1$. We can see from this equation that the positron energy is strongly correlated to the neutrino energy.

The positron and the neutron will then propagate in the detection medium, the Liquid Scintillator (LS), loosing their kinetic energy by exciting the molecule of the LS (more details in section 2.2.2). Once stopped, the positron will annihilate with an electron from the medium producing two 511 KeV gamma. Those gamma will themselves interact with the LS, exciting it before being absorbed by photoelectrical effect. The neutron will be captured by an hydrogen, emitting a 2.2 MeV gamma in the process. This gamma will also deposit its energy before being absorbed by the LS.

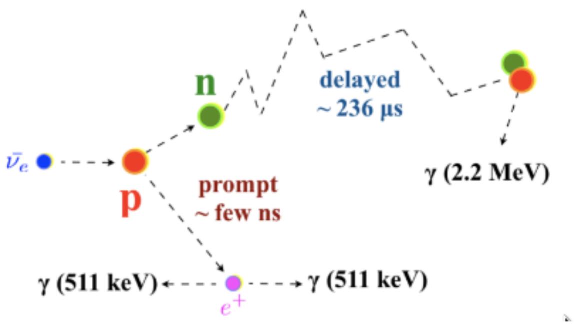

FIGURE 2.5 – Schematics of an IBD interaction in the central detector of JUNO

The scintillation photons have an UV frequency and will be captured by PMTs observing the CD. The analog signal of the PMTs digitized by the electronic is the signal of our experiment. The signal produced by the positron is subsequently called the prompt signal, and the signal coming from the neutron the delayed signal. This naming convention come from the fact that the positron will deposit its energy rather quickly (few ns) where the neutron will take a bit more time ($\sim 236\ \mu$s).

2.2.2 Central Detector (CD)

The central detector, composed of 20 ktons of Liquid Scintillator (LS), is the main part of JUNO. The LS is contained in a spherical acrylic vessel supported by a stainless steel structure. The CD and its structural support are submerged in a cylindrical water pool of 43.5m diameter and 44m height. We're confident that the water pool provide sufficient buffer protection in every direction against the rock radioactivity.

Acrylic vessel

The acrylic vessel is a spherical vessel of inner diameter of 35.4 m and a thickness of 120 mm. It is assembled from 265 acrylic panels, thermo bonded together. The acrylic recipes has been carefully tuned with extensive R&D to ensure it does not include plasticizer and anti-UV material that would stop the scintillation photons. Those panels requires to be pure of radioactive materials to not cause background. Current setup where the acrylic panels are molded in cleanrooms of class 10000, let us reach a uranium and thorium contamination of <0.5 ppt. The molding and thermoforming processes is optimized to increase the assemblage transparency in water to >96%. The acrylic vessel is supported by a stainless steel structure via supporting node (fig 2.6). The structure and the nodes are designed to be resilient to natural catastrophic events such as earthquake and can support many times the effective load of the acrylic vessel.

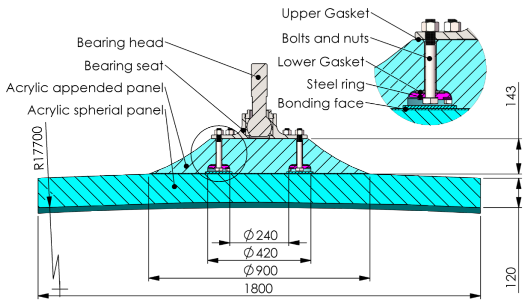

FIGURE 2.6 – Schematics of the supporting node for the acrylic vessel

Liquid scintillator

The Liquid Scintillator (LS) has a similar recipe as the one used in Daya Bay [19] but without gadolinium doping. It is made of three components, necessary to shift the wavelength of emitted photons to prevent their reabsorption:

1. The detection medium, the *linear alkylbenzene* (LAB). Selected because of its excellent transparency, high flash point, low chemical reactivity and good light yield. Accounting for $\sim$ 98% of the LS, it is the main component with which ionizing particles and gamma interact. Charged particles will collide with its electronic cloud transferring energy to the molecules, gamma will interact via compton effect with the electronic cloud before finally be absorbed via photoelectric effect.
2. The second component of the LS is the *2,5-diphenyloxazole* (PPO). A fraction of the excitation energy of the LAB is transferred to the PPO, mainly via non radiative process [20]. The PPO molecules de-excites in the same way, transferring their energy to the bis-MSB. The PPO makes for 1.5 % of the LS.
3. The last component is the *p-bis(o-methylstyryl)-benzene* (bis-MSB). Once excited by the PPO, it will emit photon with an average wavelength of $\sim$ 430 nm (full spectrum in figure 2.7) that can be detected by our photo-multipliers systems. It amount for $\sim$ 0.5% of the LS.

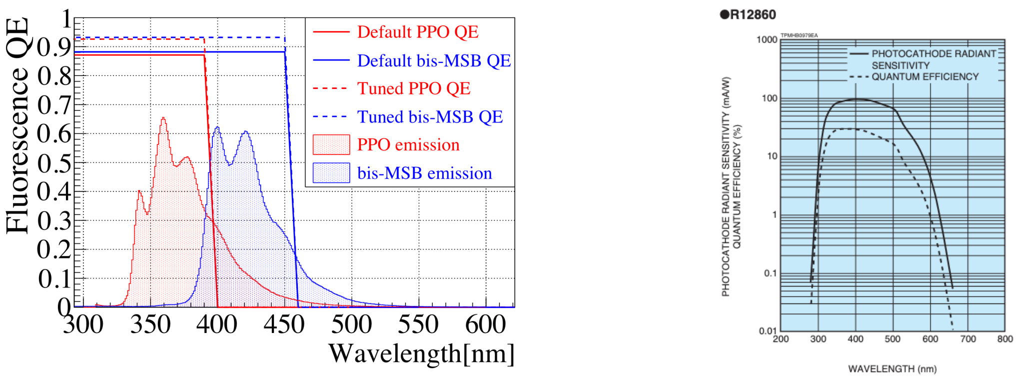

FIGURE 2.7 – **On the left:** Quantum efficiency (QE) and emission spectrum of the LAB and the bis-MSB [19]. **On the right:** Sensitivity of the Hamamatsu LPMT depending on the wavelength of the incident photons [21].

This formula has been optimized using dedicated studies with a Daya Bay detector [19, 22] to reach the requirements for the JUNO experiment:

— A light yield / MeV of the amount of 10^4 photons to maximize the statistic in the energy measurement.

— An attenuation length comparable to the size of the detector to prevent losing photons during their propagation in the LS. The final attenuation length is 25.8m [23] to compare with the CD diameter of 35.4m.

— Uranium/Thorium radiopurity to prevent background signal. The reactor neutrino program require a contamination fraction $F < 10^{-15}$ while the solar neutrino program require $F < 10^{-17}$.

The LS will frequently be purified and tested in the Online Scintillator Internal Radioactivity Investigation System (OSIRIS) [24] to ensure that the requirements are kept during the lifetime of the experiment.

Large Photo-Multipliers Tubes(LPMTs)

The scintillation light produced by the LS is then collected by Photo-Multipliers Tubes (PMT) that transform the incoming photon into an electric signal. As described in figure 2.8, the incident photons interact with the photocatode via photoelectric effect producing an electron called a Photo-Electron (PE). This PE is then focused on the dynodes where the high voltage will allow it to be multiplied. After multiple amplification the resulting charge - in coulomb [C] - is collected by the anode and the resulting electric signal can be digitalized by the readout electronics from which the charge and timing can be extracted.

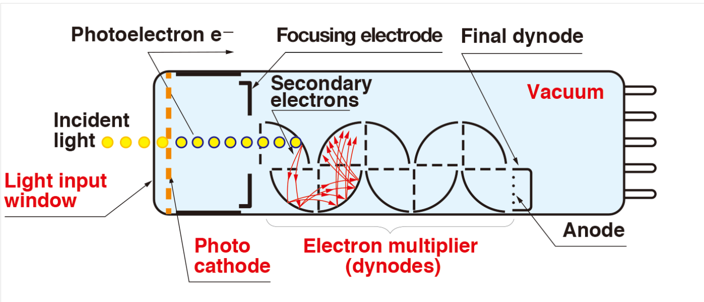

FIGURE 2.8 – Schematic of a PMT

The Large Photo-Multipliers Tubes (LPMT), used in the central detector and in the water pool, are 20-inch (50.8 cm) radius PMTs. $\sim$ 5000 dynode-PMTs [21] were produced by the Hamamatsu© company and $\sim$ 15000 Micro-Channel Plate (MCP) [25] by the NNVT© company. This system is the one responsible for the energy measurement with a energy resolution of $3\%/\sqrt{E}$, resolution necessary for the mass ordering measurement. To reach this precision, the system is composed of 17612 PMTs quasi uniformly distributed over the detector for a coverage of 75.2% reaching $\sim$ 1800 PE/MeV or $\sim$ 2.3% resolution due to statistic, leaving $\sim$ 0.7% for the systematic uncertainties. To maintain the resolution over the lifetime of the experiment, JUNO require a failure rate < 1% over 6 years.

The LPMTs electronic are divided in two parts. One "near", located underwater, in proximity of the LPMT to reduce the cable length between the PMT and early electronic. A second one, outside of the detector that is responsible for higher level analysis before sending the data to the DAQ.

The light yield per MeV induce that a LPMT can collect between 1 and 1000 PE per event, causing non linearity in the PMT response that need to be understood and calibrated, see section 2.3 for more details.

Small Photo-Multipliers Tubes (SPMTs)

The Small PMT (SPMTs) system is made of 3-inch (7.62 cm) PMTs. They will be used in the CD as a secondary detection system. Those 25600 SPMTs will observe the same events as the LPMTs, thus sharing the physics and detector systematics up until the photon conversion. With a detector coverage of 2.7%, this system will collect $\sim$ 43 PE/MeV for a final energy resolution of $\sim$ 17%. This resolution is not enough to measure the NMO, θ_{13}, Δm^2_{31} but will be sufficient to independently measure θ_{12} and Δm^2_{21}.

Due to the low PE rate, SPMTs will be running in photo-counting mode in the reactor range thus will be insensitive to non-linearity effect. Also, due to their smaller size and electronics, SPMTs have a better timing resolutions than the LPMTs. At higher energy range, like supernovae events, LPMTs will saturate where SPMTs due to their lower PE collection will to produce a reliable measure of the energy spectrum.

The Data Acquisition System (DAQ) is designed to support the event rate of IBD, background, dark noise and supplementary storage buffers are present in the LPMT electronics to withstand the event rate during supernovae burst.

2.2.3 Veto detector

The CD will be bathed in constant background noise coming from numerous sources : the radioactivity from surrounding rock and its own components or from the flux of cosmic muons. This background needs to be rejected to ensure the purity of the IBD spectrum. To prevent a big part of them, JUNO use two veto detector that will tag events as background before CD analysis.

Cherenkov in water pool

The Water Cherenkov Detector (WCD) is the instrumentalization of the water buffer around the CD. When high speed charged particles will pass through the water, they will produced cherenkov photons. The light will be collected by 2400 MCP LPMTs installed on the outer surface of the CD structure. The muons veto strategy is based on a PMT multiplicity condition. WCD PMTs are grouped in ten zones: 5 in the top, 5 in the bottom. A veto is raised either when more than 19 PMTs are triggered in one zone or when two adjacent zones simultaneously trigger more than 13 PMTs. Using this trigger, we expect to reach a muon detection efficiency of 99.5% while keeping the noise at reasonable level.

Top tracker

The JUNO Top Tracker (TT) is a plastic scintillator detector located on the top of the experiment (see figure 2.9). Made from plastic scintillator from OPERA [26] layered horizontally in 3 layers on the top of the detector, the TT will be able to detect incoming atmospheric muons. With its coverage, about 1/3 of the of all atmospheric muons that passing through the CD will also pass through the 3 layer of the detector. While it does not cover the majority of the CD, the TT is particularly effective to detect muons coming through the filling chimney region which might present difficulties from the other subsystems in some classes of events.

2.3 Calibration strategy

The calibration is a crucial part of the JUNO experiment. Because we are looking at civil reactor neutrino it might be impossible to run measurement without signal, it would need to shut down every reactor from the Taishan and Yangjiang power plants which is realistically impossible. Because of this continuous rate, low frequency signal event, we need high frequency, recognisable sources in the energy range of interest, [0-12] MeV for the positron signal and 2.2 MeV for the neutron capture. It is understood that the CD response will be different depending on the type of particle, due to the

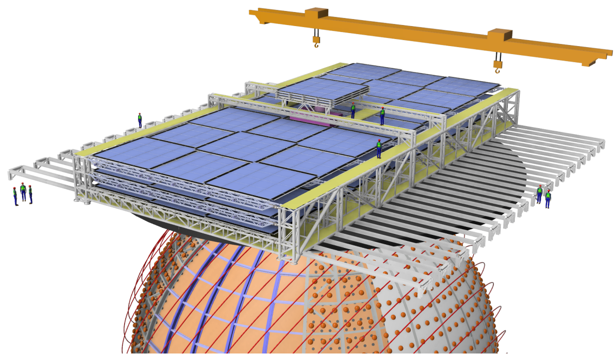

FIGURE 2.9 – The JUNO top tracker

interaction with LS, and on the position on the event, due to the absorption length of the LS and the optical response of the acrylic sphere (see section 2.5). The energy response is also expected to be non-linear due to the LS response [19] but also due to the saturation of the LPMTs system when collecting a large amount of PE [27].

2.3.1 Energy scale calibration

While electrons and positrons sources would be ideal, for a large LS detector thin-walled electrons or positrons sources could lead to leakage of radionuclides causing contamination. Instead are considered gamma sources in the range of the prompt energy of IBDs. The sources are reported in table 2.4.

Sources / Processes	Type	Radiation
^{137}Cs	γ	0.0662 MeV
^{54}Mn	γ	0.835 MeV
^{60}Co	γ	1.173 + 1.333 MeV
^{40}K	γ	1.461 MeV
^{68}Ge	e^+	annihilation 0.511 + 0.511 MeV
^{241}Am-Be	n, γ	neutron + 4.43 MeV (12C*)
^{241}Am-^{13}C	n, γ	neutron + 6.13 MeV (16O*)
$(n, \gamma)p$	γ	2.22 MeV
$(n, \gamma)^{12}$C	γ	4.94 MeV or 3.68 + 1.26 MeV

TABLE 2.4 – List of sources and their process considered for the energy scale calibration

For the ^{68}Ge source, it'll decay in ^{68}Ga via electron capture, which will itself β^+ decay into ^{68}Zn. The positrons will be absorbed by the enclosure so only the annihilation gamma will be released. In addition, (α, n) sources like ^{241}Am-Be and ^{241}Am-^{13}C are used to provide both high energy gamma and neutrons, which will later be captured in the LS producing the 2.2 MeV gamma.

From this calibration we call E_{vis} the "visible energy" that is reconstructed by our current algorithms and we compare it to the true energy deposited by the calibration source. The results shown in figure 2.10 show the expected response of the detector from calibration sources. The non-linearity is clearly visible from the E_{vis}/E_{true} shape. See [28] for more details.

2.3.2 Calibration system

The JUNO detector will need to investigate the non-uniformity in the detector response depending of the position of the event (more details in section 2.5). For this we will able to deploy sources

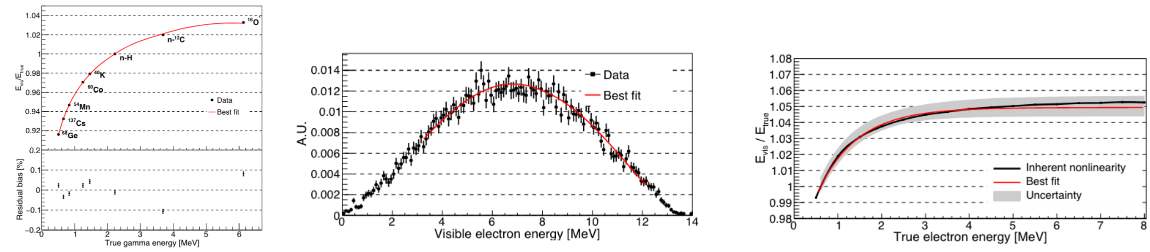

(A) Gamma non-linearity (B) Boron non-spectrum (C) Electron non-linearity

FIGURE 2.10 – Fitted and simulated non linearity of gamma and electron sources and ^{12}B spectrum. Black points are simulated data while red points are the best fit

using multiples systems that are schematized in figure 2.11 :

- For a one-dimension vertical calibration, the Automatic Calibration Unit (ACU) will be able to deploy multiple radioactive sources or a pulse laser diffuser ball along the central axis of the CD through the top chimney. The source position precision is less than 1cm.
- For off-axis calibration, a calibration source attached to a Cable Loop System (CLS) can be moved on a vertical half-plane by adjusting the length of two connection cable. Two set of CSL will be deployed to provide a 79% effective coverage of a vertical plane.
- A Guiding Tube (GT) will surround the CD to calibrate the non-uniformity of the response at the edge of the detector
- A Remotely Operated under-LS Vehicle (ROV) can be deployed to desired location inside LS for a more precise and comprehensive calibration. The ROV will also be equipped with a camera for inspection of the CD.

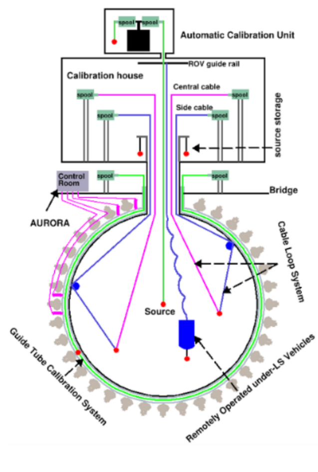

FIGURE 2.11 – Overview of the calibration system

The preliminary calibration program is depicted in table 2.5.
A partir d'ici, pas de relecture de ma part

2.4 Software

The simulation, reconstruction and analysis algorithms are all packaged in the JUNO software, subsequently called the software. It is composed of multiple components integrated in the SNiPER [29] framework:

Program	Purpose	System	Duration [min]
Weekly calibration	Neutron (Am-C)	ACU	63
	Laser	ACU	78
Monthly calibration	Neutron (Am-C)	ACU	120
	Laser	ACU	147
	Neutron (Am-C)	CLS	333
	Neutron (Am-C)	GT	73
Comprehensive calibration	Neutron (Am-C)	ACU, CLS and GT	1942
	Neutron (Am-Be)	ACU	75
	Laser	ACU	391
	^{68}Ge	ACU	75
	^{137}Cs	ACU	75
	^{54}Mn	ACU	75
	^{60}Co	ACU	75
	^{40}K	ACU	158

TABLE 2.5 – Calibration program of the JUNO experiment

— Various primary particles simulators for the different kind of events, background and calibration sources.

— A Geant4 [30–32] simulation simulating the detectors geometries, a custom optical model for the LS and the supporting structures of the detectors. The Geant4 simulation integrate all relevant physics process for JUNO, validated by the collaboration. This step of the simulation is commonly called *Detsim* and compute up to the production of photo-electrons in the PMTs. The optics properties of the different materials and detector components have been measured beforehand to be used to define the material and surfaces in the simulation

— An electronic simulation, simulating the response waveform of the PMTs, tracking it through the digitization process, accounting for effects such as non-linearity, dark noise, Time Transit Spread (TTS), pre-pulsing, after-pulsing and ringing if the waveform. This step is commonly referenced as *Elecsim*.

— A waveform reconstruction where the digitized waveform are filtered to remove high-frequency white noise and then deconvoluted to yield time and charge informations of the photons hits on the PMTs. This step is commonly referenced as *Calib*.

— The charge and time informations are used by reconstruction algorithms to reconstruct the interaction vertex and the deposited energy. This step is commonly reported as *Reco*. See section 2.5 for more details on the reconstruction.

— Once the singular events are reconstructed, they go through event pairing and classification to select IBD events. This step is named Event Classification.

— The purified signal is then analysed by the analysis framework which depend of the physics topic of interest.

The steps Reco and Event Classification are divided into two category of algorithm. Fast but less accurate algorithms that are running during the data taking designed as *Online* algorithms. Those algorithm are used to take the decision to save the event on tape or to throw it away. More accurate algorithms that run on batch of events designed *Offline* algorithms. They are used for the physics analysis and the Offline Reco will be a topic of interest for this thesis.

2.5 State of the art of the Offline IBD reconstruction in JUNO

The main reconstruction method currently run in JUNO is a data-driven method based on a likelihood maximization [33, 34] using only the LPMTs. The first step is to reconstruct the interaction vertex from which the energy reconstruction is dependent. It is also necessary for event pairing and classification.

2.5.1 Interaction vertex reconstruction

To start the likelihood maximization, a rough estimation of the vertex and of the event timing is needed. We start by estimating the vertex position using a charge based algorithm.

Charge based algorithm

The charge-based algorithm is basically base on the charge-weighted average of the PMT position.

$$\vec{r}_{cb} = a \cdot \frac{\sum_i q_i \cdot \vec{r}_i}{\sum_i q_i} \tag{2.3}$$

Where q_i is the reconstructed charge of the pulse of the ith PMT and $\vec{r}_i$ is its position. $\vec{r}_0$ is the reconstructed interaction position. a is a scale factor introduced because a weighted average over a 3D sphere is inherently biased. Using calibration we can estimate $a \approx 1.3$ [35]. The results in figure 2.12b shows that the reconstruction is biased from around 15m and further. This is due to the phenomena called "total reflection area" or TR Area.

As depicted in the figure 2.12a the optical photons, given that they have a sufficiently large incidence angle, can be deviated of their trajectories when passing through the interfaces LS-acrylic and water-acrylic due to the optical index difference. This cause photons to be lost or to be detected by PMT further than anticipated if we consider their rectilinear trajectories. This cause the charge barycenter the be located closer to the center than the vent really is.

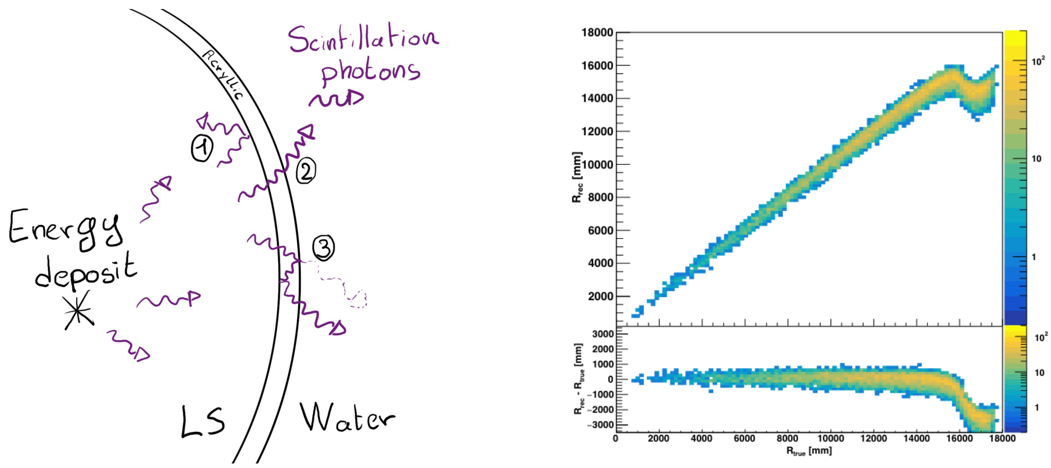

(A) Illustration of the different optical photons reflection scenarios. **1** is the reflection of the photon at the interface LS-acrylic or acrylic-water. **2** is the transmission of the photons through the interfaces. **3** is the conduction of the photon in the acrylic.

(B) Heatmap of R_{rec} and $R_{rec} - R_{true}$ as a function of R_{true} for 4MeV prompt signals uniformly distributed in the detector calculated by the charge based algorithm

FIGURE 2.12

It is to be noted that charge based algorithm, in addition to be biased near the edge of the detector, does not provide any information about the timing of the event. Therefore, a time based algorithm needs to be introduced to provide initial values.

Time based algorithm

The time based algorithm use the distribution of the time of flight corrections Δt (Eq 2.4) of an event to reconstruct its vertex and t_0. It follow the following iterations:

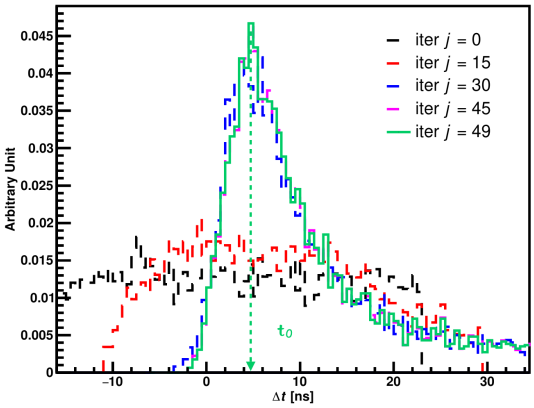

(A) Δt distribution at different iterations step j

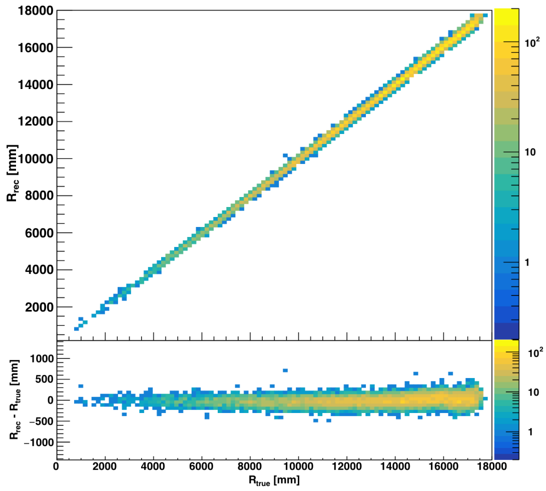

(B) Heatmap of R_{rec} and $R_{rec} - R_{true}$ as a function of R_{true} for 4MeV prompt signals uniformly distributed in the detector calculated by the time based algorithm

1. Use the charge based algorithm to get an initial vertex to start the iteration.
2. Calculate the time of flight correction for the ith PMT using

$$\Delta t_i(j) = t_i - \text{tof}_i(j) \tag{2.4}$$

   where j is the iteration step, t_i is the timing of the ith PMT, and tof_i is the time-of-flight of the photon considering an rectilinear trajectory and an effective velocity in the LS and water (see [35] for detailed description of this effective velocity). Plot the Δt distribution and label the peak position as Δt^{peak} (see fig 2.13a).
3. Calculate a correction vector $\vec{\delta}[\vec{r}(j)]$ as

$$\vec{\delta}[\vec{r}(j)] = \frac{\sum_i \left(\frac{\Delta t(j) - \Delta t^{\text{peak}}(j)}{\text{tof}_i(j)}\right) \cdot (\vec{r}_0(j) - \vec{r}_i)}{N^{\text{peak}}(j)} \tag{2.5}$$

   where $\vec{r}_0$ is the vertex position at the beginning of this iteration, $\vec{r}_i$ is the position of the ith PMT. To minimize the effect of scattering, dark noise and reflection, only the pulse happening in a time window (-10 ns, +5 ns) around Δt^{peak} are considered. N^{peak} is the number of PE collected in this time-window.
4. if $\vec{\delta}[\vec{r}(j)] < 1\text{mm}$ or $j \geq 100$, stop the iteration. Otherwise $\vec{r}_0(j+1) = \vec{r}_0(j) + \vec{\delta}[\vec{r}(j)]$ and go to step 2.

However because the earliest arrival time is used, t_i is related to the number photoelectrons N_i^{pe} detected by the PMT [36–38]. To reduce bias in the vertex reconstruction, the following equation is used to correct t_i into t_i':

$$t_i' = t_i - p_0/\sqrt{N_i^{\text{pe}}} - p_1 - p_2/N_i^{\text{pe}} \tag{2.6}$$

The parameters (p_0, p_1, p_2) were optimized to (9.42, 0.74, -4.60) for Hamamatsu PMTs and (41.31, -12.04, -20.02) for NNVT PMTs [35]. The results presented in figure 2.13b shows that the time based algorithm provide a more accurate vertex and is unbiased even in the TR area. This results $(\vec{r}_0, t_0)$ is used as initial value for the likelihood algorithm.

Time likelihood algorithm

The time likelihood algorithm use the residual time expressed as follow

$$t^i_{\text{res}}(\vec{r}_0, t_0) = t_i - \text{tof}_i - t_0 \tag{2.7}$$

In a first order approximation, the scintillator response Probability Density Function (PDF) can be described as the emission time profile of the scintillation photons, the Time Transit Spread (TTS) and the dark noise of the PMTs. The emission time profile $f(t_{\text{res}})$ is described like

$$f(t_{\text{res}}) = \sum_k \frac{\rho_k}{\tau_k} e^{\frac{-t_{\text{res}}}{\tau_k}}\,,\ \sum_k \rho_k = 1 \tag{2.8}$$

as the sum of the k component that emit light in the LS each one characterised by it's decay time τ_k and intensity fraction ρ_k. The TTS component is expressed as a gaussian convolution

$$g(t_{\text{res}}) = \frac{1}{\sqrt{2\pi}\sigma} e^{\frac{-(t_{\text{res}}-\nu)^2}{2\sigma^2}} \cdot f(t_{\text{res}}) \tag{2.9}$$

where σ is the TTS of PMTs and ν is the average transit time. The dark noise is not correlated with any physical events and considered as constant rate over the time window considered T. By normalizing the dark noise probability $\epsilon(t_{\text{res}})$ as $\int_T \epsilon(t_{\text{res}}) dt_{\text{res}} = \epsilon_{\text{dn}}$, it can be integrated in the PDF as

$$p(t_{\text{res}}) = (1 - \epsilon_{\text{dn}}) \cdot g(t_{\text{res}}) + \epsilon(t_{\text{res}}) \tag{2.10}$$

The distribution of the residual time t_{res} of an event can then be compared to $p(t_{\text{res}})$ and the best fitting vertex $\vec{r}_0$ and t_0 can be chosen by minimizing

$$\mathcal{L}(\vec{r}_0, t_0) = -\ln\left(\prod_i p(t^i_{\text{res}})\right) \tag{2.11}$$

2.5.2 Energy reconstruction

2.5.3 Particle identification

2.5.4 Machine learning for reconstruction

Vertex reconstruction

Energy reconstruction

2.6 JUNO sensitivity to NMO and precise measurements

2.6.1 Fitting procedure

Chapter 3

Machine learning and Artificial Neural Network

3.1 History of the Machine learning

3.2 Boosted Decision Tree (BDT)

3.3 Artificial Neural Network (NN)

3.3.1 Fully Connected Deep Neural Network (FCDNN)

3.3.2 Convolutional Neural Network (CNN)

3.3.3 Graph Neural Network (GNN)

3.3.4 Adversorial Neural Network (ANN)

Generative Adversorial Network (GAN)

Reinformcement Learning (RL)

Random Search (RS)

Bayesian Optimization

Chapter 4

Image recognition for IBD reconstruction with the SPMT system

Chapter 5

Graph representation of JUNO for IBD reconstruction with the LPMT system

Chapter 6

Reliability of machine learning methods

Chapter 7

Discrimination of e+/e- events in JUNO

Chapter 8

Conclusion

Bibliography

[1] Liang Zhan, Yifang Wang, Jun Cao, and Liangjian Wen. "Determination of the Neutrino Mass Hierarchy at an Intermediate Baseline". *Physical Review D* 78.11 (Dec. 10, 2008), 111103. ISSN: 1550-7998, 1550-2368. DOI: 10.1103/PhysRevD.78.111103. eprint: 0807.3203[hep-ex, physics:hep-ph]. URL: http://arxiv.org/abs/0807.3203 (visited on 09/18/2023).

[2] Fengpeng An et al. "Neutrino Physics with JUNO". *Journal of Physics G: Nuclear and Particle Physics* 43.3 (Mar. 1, 2016), 030401. ISSN: 0954-3899, 1361-6471. DOI: 10.1088/0954-3899/43/3/030401. eprint: 1507.05613[hep-ex,physics:physics]. URL: http://arxiv.org/abs/1507.05613 (visited on 07/28/2023).

[3] Liang Zhan, Yifang Wang, Jun Cao, and Liangjian Wen. "Experimental Requirements to Determine the Neutrino Mass Hierarchy Using Reactor Neutrinos". *Physical Review D* 79.7 (Apr. 14, 2009), 073007. ISSN: 1550-7998, 1550-2368. DOI: 10.1103/PhysRevD.79.073007. eprint: 0901.2976[hep-ex]. URL: http://arxiv.org/abs/0901.2976 (visited on 09/18/2023).

[4] A. A. Hahn, K. Schreckenbach, W. Gelletly, F. von Feilitzsch, G. Colvin, and B. Krusche. "Antineutrino spectra from 241Pu and 239Pu thermal neutron fission products". *Physics Letters B* 218.3 (Feb. 23, 1989), 365–368. ISSN: 0370-2693. DOI: 10.1016/0370-2693(89)91598-0. URL: https://www.sciencedirect.com/science/article/pii/0370269389915980 (visited on 01/16/2024).

[5] Th A. Mueller et al. "Improved Predictions of Reactor Antineutrino Spectra". *Physical Review C* 83.5 (May 23, 2011), 054615. ISSN: 0556-2813, 1089-490X. DOI: 10.1103/PhysRevC.83.054615. eprint: 1101.2663[hep-ex, physics:nucl-ex]. URL: http://arxiv.org/abs/1101.2663 (visited on 01/16/2024).

[6] F. von Feilitzsch, A. A. Hahn, and K. Schreckenbach. "Experimental beta-spectra from 239Pu and 235U thermal neutron fission products and their correlated antineutrino spectra". *Physics Letters B* 118.1 (Dec. 2, 1982), 162–166. ISSN: 0370-2693. DOI: 10.1016/0370-2693(82)90622-0. URL: https://www.sciencedirect.com/science/article/pii/0370269382906220 (visited on 01/16/2024).

[7] K. Schreckenbach, G. Colvin, W. Gelletly, and F. Von Feilitzsch. "Determination of the antineutrino spectrum from 235U thermal neutron fission products up to 9.5 MeV". *Physics Letters B* 160.4 (Oct. 10, 1985), 325–330. ISSN: 0370-2693. DOI: 10.1016/0370-2693(85)91337-1. URL: https://www.sciencedirect.com/science/article/pii/0370269385913371 (visited on 01/16/2024).

[8] Patrick Huber. "On the determination of anti-neutrino spectra from nuclear reactors". *Physical Review C* 84.2 (Aug. 29, 2011), 024617. ISSN: 0556-2813, 1089-490X. DOI: 10.1103/PhysRevC.84.024617. eprint: 1106.0687[hep-ex,physics:hep-ph,physics:nucl-ex,physics:nucl-th]. URL: http://arxiv.org/abs/1106.0687 (visited on 01/16/2024).

[9] P. Vogel, G. K. Schenter, F. M. Mann, and R. E. Schenter. "Reactor antineutrino spectra and their application to antineutrino-induced reactions. II". *Physical Review C* 24.4 (Oct. 1, 1981). Publisher: American Physical Society, 1543–1553. DOI: 10.1103/PhysRevC.24.1543. URL: https://link.aps.org/doi/10.1103/PhysRevC.24.1543 (visited on 01/16/2024).

[10] D. A. Dwyer and T. J. Langford. "Spectral Structure of Electron Antineutrinos from Nuclear Reactors". *Physical Review Letters* 114.1 (Jan. 7, 2015), 012502. ISSN: 0031-9007, 1079-7114. DOI: 10.1103/PhysRevLett.114.012502. eprint: 1407.1281[hep-ex,physics:nucl-ex]. URL: http://arxiv.org/abs/1407.1281 (visited on 01/16/2024).

[11] JUNO Collaboration et al. "Sub-percent Precision Measurement of Neutrino Oscillation Parameters with JUNO". *Chinese Physics C* 46.12 (Dec. 1, 2022), 123001. ISSN: 1674-1137, 2058-6132. DOI: 10.1088/1674-1137/ac8bc9. eprint: 2204.13249[hep-ex]. URL: http://arxiv.org/abs/2204.13249 (visited on 08/11/2023).

[12] JUNO Collaboration et al. *TAO Conceptual Design Report: A Precision Measurement of the Reactor Antineutrino Spectrum with Sub-percent Energy Resolution*. May 18, 2020. DOI: 10.48550/arXiv.2005.08745. eprint: 2005.08745[hep-ex,physics:nucl-ex,physics:physics]. URL: http://arxiv.org/abs/2005.08745 (visited on 01/18/2024).

[13] G. Mention, M. Fechner, Th. Lasserre, Th. A. Mueller, D. Lhuillier, M. Cribier, and A. Letourneau. "Reactor antineutrino anomaly". *Physical Review D* 83.7 (Apr. 29, 2011). Publisher: American Physical Society, 073006. DOI: 10.1103/PhysRevD.83.073006. URL: https://link.aps.org/doi/10.1103/PhysRevD.83.073006 (visited on 03/05/2024).

[14] V. Kopeikin, M. Skorokhvatov, and O. Titov. "Reevaluating reactor antineutrino spectra with new measurements of the ratio between ^{235}U and ^{239}Pu β spectra". *Physical Review D* 104.7 (Oct. 25, 2021), L071301. ISSN: 2470-0010, 2470-0029. DOI: 10.1103/PhysRevD.104.L071301. eprint: 2103.01684[hep-ph,physics:nucl-ex,physics:nucl-th]. URL: http://arxiv.org/abs/2103.01684 (visited on 01/18/2024).

[15] A. Letourneau et al. "On the origin of the reactor antineutrino anomalies in light of a new summation model with parameterized β^- transitions". *Physical Review Letters* 130.2 (Jan. 10, 2023), 021801. ISSN: 0031-9007, 1079-7114. DOI: 10.1103/PhysRevLett.130.021801. eprint: 2205.14954[hep-ex,physics:hep-ph]. URL: http://arxiv.org/abs/2205.14954 (visited on 01/16/2024).

[16] Particle Data Group et al. "Review of Particle Physics". *Progress of Theoretical and Experimental Physics* 2020.8 (Aug. 14, 2020), 083C01. ISSN: 2050-3911. DOI: 10.1093/ptep/ptaa104. URL: https://doi.org/10.1093/ptep/ptaa104 (visited on 12/04/2023).

[17] Super-Kamiokande Collaboration et al. "Diffuse Supernova Neutrino Background Search at Super-Kamiokande". *Physical Review D* 104.12 (Dec. 10, 2021), 122002. ISSN: 2470-0010, 2470-0029. DOI: 10.1103/PhysRevD.104.122002. eprint: 2109.11174[astro-ph,physics:hep-ex]. URL: http://arxiv.org/abs/2109.11174 (visited on 02/28/2024).

[18] Alessandro Strumia and Francesco Vissani. "Precise quasielastic neutrino/nucleon cross section". *Physics Letters B* 564.1 (July 2003), 42–54. ISSN: 03702693. DOI: 10.1016/S0370-2693(03)00616-6. eprint: astro-ph/0302055. URL: http://arxiv.org/abs/astro-ph/0302055 (visited on 01/16/2024).

[19] Daya Bay et al. *Optimization of the JUNO liquid scintillator composition using a Daya Bay antineutrino detector*. July 1, 2020. DOI: 10.48550/arXiv.2007.00314. eprint: 2007.00314[hep-ex,physics:physics]. URL: http://arxiv.org/abs/2007.00314 (visited on 07/26/2023).

[20] J. B. Birks. "CHAPTER 3 - THE SCINTILLATION PROCESS IN ORGANIC MATERIALS—I". *The Theory and Practice of Scintillation Counting*. Ed. by J. B. Birks. International Series of Monographs in Electronics and Instrumentation. Jan. 1, 1964, 39–67. ISBN: 978-0-08-010472-0. DOI: 10.1016/B978-0-08-010472-0.50008-2. URL: https://www.sciencedirect.com/science/article/pii/B9780080104720500082 (visited on 02/07/2024).

[21] *Photomultiplier tube R12860 | Hamamatsu Photonics*. URL: https://www.hamamatsu.com/eu/en/product/optical-sensors/pmt/pmt_tube-alone/head-on-type/R12860.html (visited on 02/08/2024).

[22] Yan Zhang, Ze-Yuan Yu, Xin-Ying Li, Zi-Yan Deng, and Liang-Jian Wen. "A complete optical model for liquid-scintillator detectors". *Nuclear Instruments and Methods in Physics Research Section A: Accelerators, Spectrometers, Detectors and Associated Equipment* 967 (July 2020), 163860. ISSN: 01689002. DOI: 10.1016/j.nima.2020.163860. eprint: 2003.12212[physics]. URL: http://arxiv.org/abs/2003.12212 (visited on 02/07/2024).

[23] Hai-Bo Yang et al. "Light Attenuation Length of High Quality Linear Alkyl Benzene as Liquid Scintillator Solvent for the JUNO Experiment". *Journal of Instrumentation* 12.11 (Nov. 27, 2017), T11004–T11004. ISSN: 1748-0221. DOI: 10.1088/1748-0221/12/11/T11004. eprint: 1703.01867[hep-ex,physics:physics]. URL: http://arxiv.org/abs/1703.01867 (visited on 07/28/2023).

[24] JUNO Collaboration et al. *The Design and Sensitivity of JUNO's scintillator radiopurity pre-detector OSIRIS*. Mar. 31, 2021. DOI: 10.48550/arXiv.2103.16900. eprint: 2103.16900[physics]. URL: http://arxiv.org/abs/2103.16900 (visited on 02/07/2024).

[25] Angel Abusleme et al. "Mass Testing and Characterization of 20-inch PMTs for JUNO". *The European Physical Journal C* 82.12 (Dec. 24, 2022), 1168. ISSN: 1434-6052. DOI: 10.1140/epjc/s10052-022-11002-8. eprint: 2205.08629[hep-ex,physics:physics]. URL: http://arxiv.org/abs/2205.08629 (visited on 02/08/2024).

[26] R. Acquafredda et al. "The OPERA experiment in the CERN to Gran Sasso neutrino beam". *Journal of Instrumentation* 4.4 (Apr. 2009), P04018. ISSN: 1748-0221. DOI: 10.1088/1748-0221/4/04/P04018. URL: https://dx.doi.org/10.1088/1748-0221/4/04/P04018 (visited on 02/29/2024).

[27] Yang Han. "Dual Calorimetry for High Precision Neutrino Oscillation Measurement at JUNO Experiment". AstroParticule et Cosmologie, France, Paris U. VII, APC, Not specified, June 2021.

[28] JUNO collaboration et al. "Calibration Strategy of the JUNO Experiment". *Journal of High Energy Physics* 2021.3 (Mar. 2021), 4. ISSN: 1029-8479. DOI: 10.1007/JHEP03(2021)004. eprint: 2011.06405[hep-ex,physics:physics]. URL: http://arxiv.org/abs/2011.06405 (visited on 08/10/2023).

[29] Tao Lin et al. "The Application of SNiPER to the JUNO Simulation". *Journal of Physics: Conference Series* 898.4 (Oct. 2017). Publisher: IOP Publishing, 042029. ISSN: 1742-6596. DOI: 10.1088/1742-6596/898/4/042029. URL: https://dx.doi.org/10.1088/1742-6596/898/4/042029 (visited on 02/27/2024).

[30] S. Agostinelli et al. "Geant4—a simulation toolkit". *Nuclear Instruments and Methods in Physics Research Section A: Accelerators, Spectrometers, Detectors and Associated Equipment* 506.3 (July 1, 2003), 250–303. ISSN: 0168-9002. DOI: 10.1016/S0168-9002(03)01368-8. URL: https://www.sciencedirect.com/science/article/pii/S0168900203013688 (visited on 02/27/2024).

[31] J. Allison et al. "Geant4 developments and applications". *IEEE Transactions on Nuclear Science* 53.1 (Feb. 2006). Conference Name: IEEE Transactions on Nuclear Science, 270–278. ISSN: 1558-1578. DOI: 10.1109/TNS.2006.869826. URL: https://ieeexplore.ieee.org/document/1610988?isnumber=33833&arnumber=1610988&count=33&index=7 (visited on 02/27/2024).

[32] J. Allison et al. "Recent developments in Geant4". *Nuclear Instruments and Methods in Physics Research Section A: Accelerators, Spectrometers, Detectors and Associated Equipment* 835 (Nov. 1, 2016), 186–225. ISSN: 0168-9002. DOI: 10.1016/j.nima.2016.06.125. URL: https://www.sciencedirect.com/science/article/pii/S0168900216306957 (visited on 02/27/2024).

[33] Wenjie Wu, Miao He, Xiang Zhou, and Haoxue Qiao. "A new method of energy reconstruction for large spherical liquid scintillator detectors". *Journal of Instrumentation* 14.3 (Mar. 8, 2019), P03009–P03009. ISSN: 1748-0221. DOI: 10.1088/1748-0221/14/03/P03009. eprint: 1812.01799[hep-ex,physics:physics]. URL: http://arxiv.org/abs/1812.01799 (visited on 07/28/2023).

[34] Guihong Huang et al. "Improving the energy uniformity for large liquid scintillator detectors". *Nuclear Instruments and Methods in Physics Research Section A: Accelerators, Spectrometers, Detectors and Associated Equipment* 1001 (June 11, 2021), 165287. ISSN: 0168-9002. DOI: 10.1016/j.nima.2021.165287. URL: https://www.sciencedirect.com/science/article/pii/S0168900221002710 (visited on 03/01/2024).

[35] Ziyuan Li et al. "Event vertex and time reconstruction in large volume liquid scintillator detector". *Nuclear Science and Techniques* 32.5 (May 2021), 49. ISSN: 1001-8042, 2210-3147. DOI: 10.1007/s41365-021-00885-z. eprint: 2101.08901[hep-ex,physics:physics]. URL: http://arxiv.org/abs/2101.08901 (visited on 07/28/2023).

[36] Gioacchino Ranucci. "An analytical approach to the evaluation of the pulse shape discrimination properties of scintillators". *Nuclear Instruments and Methods in Physics Research Section A: Accelerators, Spectrometers, Detectors and Associated Equipment* 354.2 (Jan. 30, 1995), 389–399. ISSN: 0168-9002. DOI: 10.1016/0168-9002(94)00886-8. URL: https://www.sciencedirect.com/science/article/pii/0168900294008868 (visited on 03/07/2024).

[37] C. Galbiati and K. McCarty. "Time and space reconstruction in optical, non-imaging, scintillator-based particle detectors". *Nuclear Instruments and Methods in Physics Research Section A: Accelerators, Spectrometers, Detectors and Associated Equipment* 568.2 (Dec. 1, 2006), 700–709. ISSN: 0168-9002. DOI: 10.1016/j.nima.2006.07.058. URL: https://www.sciencedirect.com/science/article/pii/S0168900206013519 (visited on 03/07/2024).

[38] M. Moszyński and B. Bengtson. "Status of timing with plastic scintillation detectors". *Nuclear Instruments and Methods* 158 (Jan. 1, 1979), 1–31. ISSN: 0029-554X. DOI: 10.1016/S0029-554X(79)90170-8. URL: https://www.sciencedirect.com/science/article/pii/S0029554X79901708 (visited on 03/07/2024).